ORIGINAL ARTICLE

Hepatocyte-specific RAP1B deficiency ameliorates high-fat diet-induced obesity and liver inflammation in mice

Yinxu Fu PhD [1,2,3] | Pingyi Hu MMed [1] | Yanyang Hu MMed [1] |
Yu Fang MMed [1] | Yaping Zhou MMed [2] | Yu Shi MMed [2] |
Kaiqiang Yang MMed [2] | Ting Fu MMed [1] | Weijia Li PhD [1,4] |
Evgeniy Rostislavovich Gritskevitch PhD [4] | Liqin Jin PhD [5] | Jianxin Lyu PhD [1,2,3,5] |
Qiongya Zhao PhD [1,3,5]

[1]School of Laboratory Medicine and Bioengineering, Hangzhou Medical College, Hangzhou, China

[2]School of Laboratory Medicine and Life Sciences, Wenzhou Medical University, Wenzhou, China

[3]Key Laboratory of Laboratory Medicine, Ministry of Education, Zhejiang Provincial Key Laboratory of Medical Genetics, College of Laboratory Medicine and Life Sciences, Wenzhou Medical University, China

[4]International Sakharov Environmental Institute, Belarusian State University, Minsk, Republic of Belarus

[5]Zhejiang Provincial People's Hospital, Affiliated People's Hospital, Hangzhou Medical College, Hangzhou, China

Correspondence
Jianxin Lyu and Qiongya Zhao, School of Laboratory Medicine and Bioengineering, Hangzhou Medical College, Hangzhou, Zhejiang, China.
Email: jxlu313@163.com and qiongyazhao@gmail.com

Abstract

Aim: This study investigated the role of RAP1B in hepatic lipid metabolism and its implications in obesity and associated metabolic disorders, focusing on the molecular mechanisms through which RAP1B influences lipid accumulation, inflammation and oxidative stress in liver tissues and hepatocyte cell lines.

Materials and Methods: Liver-specific RAP1B-knockout (LKO) and overexpression (OE) mice were generated and fed a high-fat diet for 18 weeks to evaluate systemic and hepatic metabolic changes. Comprehensive metabolic phenotyping included measurements of body weight, body fat content, activity levels, energy expenditure (EE), respiratory exchange ratio (RER), glucose tolerance test and insulin tolerance test. RAP1B-knockdown AML12 hepatocytes were used for in vitro studies. Comprehensive transcriptome and metabolome analyses identified differentially expressed genes and key metabolic shifts. Biochemical and histological analyses were performed to assess lipid accumulation, oxidative stress and inflammatory markers.

Results: We found that LKO mice exhibited significant reductions in body weight, fat pad size and liver mass, along with decreased hepatic lipid accumulation due to enhanced lipid breakdown. These mice demonstrated improved glucose tolerance and insulin sensitivity without changes in food intake. Liver histology showed reduced F4/80-positive macrophage infiltration, indicating decreased inflammatory cell recruitment. Additionally, markers of oxidative stress were significantly lower, and molecular analysis revealed downregulation of the MAPK(p38) and NF-κB signaling pathways, further supporting an anti-inflammatory hepatic environment. In contrast, OE mice showed increased liver weight, aggravated hepatic lipid accumulation

driven by enhanced lipogenesis, worsened insulin resistance and elevated inflammation.

Conclusions: This study highlights RAP1B's pivotal role in hepatic metabolism and positions it as a potential therapeutic target for obesity and related metabolic disorders.

1 | INTRODUCTION

Obesity has escalated into a global epidemic, affecting over 650 million adults and 340 million children and adolescents worldwide. This issue is propelled by many factors, including a sedentary lifestyle, poor dietary habits and genetic predisposition.[1] As a major risk factor for various metabolic disorders, obesity is intricately linked to the development of metabolic dysfunction-associated fatty liver disease (MAFLD), previously known as non-alcoholic fatty liver disease (NAFLD).[2] In individuals with obesity, excess adiposity disrupts lipid metabolism, leading to lipid accumulation in the liver (hepatic steatosis). This accumulation impairs normal liver function; is a potent catalyst for insulin resistance, type 2 diabetes and cardiovascular diseases; and is a pivotal determinant of liver-related metabolic disorders.[3]

Liver lipid accumulation is associated with inflammation and oxidative stress.[4] As lipids accumulate in hepatocytes, they cause an increase in oxidative stress owing to the elevated production of reactive oxygen species (ROS). These ROS induce lipid peroxidation, damaging cellular components and inciting further inflammation.[5,6] Chronic inflammation then perpetuates oxidative stress, forging a deleterious cycle that propels disease progression from simple steatosis to more severe liver diseases such as steatohepatitis and fibrosis.[7] This escalation is often exacerbated by the upregulation of pro-inflammatory cytokines and the recruitment of immune cells such as macrophages, which intensify the inflammatory milieu.[8] Conditions such as obesity, type 2 diabetes and metabolic syndrome are also characterized by inflammation.[9–11] As noted in recent studies, hepatic steatosis is commonly observed in these conditions, and the associated inflammation exacerbates disease progression.[12] The intricate interplay between lipid metabolism, oxidative stress and inflammation underpins the pathogenesis of liver diseases associated with obesity and metabolic disorders.

RAP1B, a member of the small GTPase family, is integral to cellular processes including adhesion, growth and differentiation.[13–15] RAP1B plays a crucial role in regulating neutrophil inflammation by preventing excessive acidity.[16] Emerging research suggests alterations in RAP1B expression in tissues from obese individuals, and RAP1B has been shown to influence mitochondrial integrity and apoptosis in renal tubular cells under high glucose conditions, suggesting its involvement in metabolic disturbances that are typical of obesity.[17,18] However, the precise mechanisms through which RAP1B modulates hepatic lipid metabolism, inflammatory responses and oxidative stress are poorly understood. Therefore, this study aimed to delineate the role of RAP1B in these processes, with a focus on its impact on energy expenditure (EE), lipid accumulation, inflammation and oxidative stress. By investigating these dynamics, we sought to elucidate the regulatory functions of RAP1B in liver metabolism and its potential as a therapeutic target for treating metabolic liver diseases.

2 | MATERIALS AND METHODS

2.1 | Animals and ethics statement

C57BL/6 mice harbouring *Rap1b* flox/− mice (C57BL/6JCya-*Rap1b*em1-flox/Cya) and *Albumin*-Cre mice were obtained from Cyagen Biosciences Inc. (Suzhou, Jiangsu, China). The liver-specific *Rap1b*-deficient (*Rap1b* flox/flox *Alb* cre, LKO) and control (*Rap1b* flox/flox, fl/fl) mice used in the experiment were produced by crossbreeding *Rap1b* flox/− mice with *Albumin*-Cre mice. In the resulting LKO mice, exon 5 and exon 6 of the *Rap1b* gene were specifically excised in the liver, ensuring targeted and tissue-specific deletion. To achieve liver-specific RAP1B OE, mice were intraperitoneally injected at 6 weeks of age with adeno-associated virus 8 (AAV8) carrying full-length RAP1B cDNA (ViGene Biosciences, Shandong, China), while control mice received AAV8 with an empty vector. Male mice aged 6–8 weeks were fed a high-fat diet (HFD; Research Diets D12492) for a minimum of 18 weeks. Four-week-old male DB/DB (C57BLKS/J-*lepr*db/*lepr*db) mice and their non-diabetic DB/m littermates were obtained from the Laboratory Animal Center of Hangzhou Medical College (Hangzhou, China). All animals were maintained in SPF-grade barriers with unrestricted access to food and water, adhering to a 12-h light/dark cycle at a temperature of 22 ± 2°C. The mice were housed in groups of 4–5 per cage from 4 weeks of age, with weekly monitoring of body weight. Tail snips were collected and genotyped. Euthanasia was performed using 1.25% tribromoethanol (0.02 mL/g body weight, intraperitoneally), after which tissues and blood were collected. Ethical approval (approval number: ZJCLA-IACUC-20020083) was granted by the Ethics Committee of Laboratory Animal Care and Welfare, Hangzhou Medical College, and all procedures complied with established principles of animal welfare and ethics.

2.2 | Cell culture

The immortalized mouse hepatocyte cell line AML12 was acquired from the Cell Bank of the Chinese Academy of Sciences, Shanghai, China and cultured at 37°C in a 5% CO_2 atmosphere. The culture medium consisted of Dulbecco's Modified Eagle's Medium/Ham's F-12 (Corning, Shanghai, China) supplemented with 12% bovine calf serum (D6429, Sigma-Aldrich, St. Louis, MO, USA), 5.5 µg/mL transferrin (T8158, Sigma-Aldrich), 10 µg/mL insulin (abs42019847, Absin, Shanghai, China), 40 ng/mL dexamethasone (A601187-0005, Sangon, Shanghai, China), 5 ng/mL sodium selenite (S5261, Sigma-Aldrich) and 1% penicillin–streptomycin–gentamicin solution (abs9245, Absin, Shanghai, China). The cells were serum-starved for 6 h before exposure to 200-µM Palmitic acid or BSA as a vehicle for at least 16 h. For the knockdown of RAP1B, pLKO-1 plasmids targeting *Rap1b* (shRNA1 for CDS: CTACGATAGAAGATTCTTAT; shRNA2 for UTR: GCTTTGATTAACACAGCTAT) were constructed by Tsingke (Hangzhou, China) and were used to produce lentiviral particles in 293-FT cells. Following the infection, AML12 cells were selected for puromycin resistance.

2.3 | RNA extraction and real-time quantitative PCR (qRT-PCR)

Total RNA was extracted from liver tissues and AML12 cells using TRIzol reagent (#15596018, Invitrogen). cDNA was synthesized using the HiScript II Q RT SuperMix kit (R222, Vazyme), and gene expression was quantified by real-time PCR using the ChamQ Universal SYBR Mix kit (Q311, Vazyme). β-Actin served as the internal control. The primers used are listed in Table S1.

2.4 | Western blotting (WB) and antibodies

Tissues and cells were lysed using RIPA buffer (MA0151, Meilune) containing protease (ST507, Beyotime) and phosphatase inhibitors (5870S, Cell Signalling Technology). The lysates were centrifuged, and the supernatant's protein concentration was determined using the Pierce™ BCA Protein Assay Kit (23225, Thermo Fisher Scientific). Proteins were separated by sodium dodecyl sulphate-polyacrylamide gel electrophoresis and transferred to PVDF membranes, which were then blocked and incubated with primary and secondary antibodies. Visualization was performed using a chemiluminescent substrate. The antibodies used are listed in Table S2.

2.5 | Metabolic caging analysis

The mice were individually housed in metabolic cages (PhenoMaster, TSE-System, Germany) for 7 days to monitor oxygen consumption and carbon dioxide production. Data from days 3 to 5 were used to calculate the respiratory exchange rate (RER) and EE. Food intake was continuously monitored using an integrated weighing sensor. Mouse activity was assessed in an open-field test using a SMART 3.0 Video Tracking System. Body composition was determined using EchoMRI (Houston, TX, USA), according to the manufacturer's instructions. Indirect calorimetry was performed following a regression-based analysis with lean mass as a covariate for normalization.[19,20]

2.6 | Glucose tolerance test (GTT) and insulin tolerance test (ITT)

Metabolic assessments including GTT and ITT were performed in the male mice. For the GTT, the mice were fasted overnight and received an intraperitoneal injection of 1 g/kg D-(+)-glucose (V900392, Sigma). Blood glucose levels were measured at specified intervals post-injection using a blood glucose meter (580; Yuwell). Blood sampling for glucose measurements was performed using sterile scissors to carefully remove approximately 1 mm from the tip of the tail, discarding the first drop and collecting the second drop of blood, approximately 10 µL. For the ITT, after a 4-h fast, the mice were administered insulin (4089, Pythonbio) at 1 U/kg, and blood glucose was similarly monitored.

2.7 | Biochemical assays

Tissue samples were homogenized at a 9:1 (volume:weight) ratio of homogenization medium to tissue. The tissue was homogenized using a mechanical homogenizer (KZ-II-F, Servicebio), following the manufacturer's instructions. The homogenate was centrifuged, and the supernatant was collected for biochemical assays. Cell disruption was performed using ultrasonic methods (300 W, 3–5 s per pulse, 30-s intervals, repeated 3–5 times). Serum was prepared by centrifuging blood samples at 4°C for 10 min at $1200 \times g$. The assay kits used were triglyceride (TG, A110-1-1), non-esterified free fatty acids (NEFA, A042-2-1), glycerol (F005-1-1) and Insulin (H203-1-2) from Nanjing Jiancheng Bioengineering Institute.

2.8 | Histology and Immunohistochemistry

The tissue samples were fixed in paraformaldehyde, dehydrated in an ethanol series, cleared in xylene and embedded in paraffin. Sections of 4–5 µm were prepared using a microtome (Leica), stained with an H&E staining kit (C0105S, Beyotime), mounted with coverslips using neutral resin (10004160, Sinopharm) and analysed microscopically. For the immunohistochemistry analysis, the sections were incubated with an F4/80 primary antibody (GB113373, Servicebio), followed by a biotinylated secondary antibody, and developed using a DAB detection kit. To prepare snap-frozen tissue blocks, tissues were dehydrated with 30% (w/v) sucrose (V900116, Sigma) for 48 h and subsequently frozen in Tissue-Tek O.C.T Compound (4583–1, SAKURA) using a Cryostat Microm HM 525 (Thermo Fisher Scientific).

2.9 | Oil Red O staining

To show lipid deposition in vitro and in vivo, the snap-frozen liver tissue blocks were sectioned into 10-μm-thick slices and subjected to 0.5% Oil Red O staining to detect lipid accumulation. In parallel, the cells in a 6-well plate were accordingly fixed with 4% (w/v) paraformaldehyde and were also stained with 0.5% Oil Red O to assess lipid droplet formation. Both the liver tissue and cultured cells were counterstained with haematoxylin. Red lipid droplets were observed under a microscope at 100/400× magnification.

2.10 | Antioxidant assay

The catalase (CAT) levels in the AML12 cells were measured using assay kits (S0051) from the Beyotime Institute of Biotechnology (Shanghai, China). Malondialdehyde (MDA) levels in the AML12 cells were also measured using assay kits (A003-4-1; Nanjing Jiancheng Bioengineering Institute). The cells were cultured and harvested following standard protocols for sample preparation and absorbance measurements.

2.11 | Transcriptome sequencing of AML12 cells

Total RNA was extracted from AML12 cells using the TRIzol reagent and sent to Novogene (Beijing, China). RNA integrity was assessed using the RNA Nano 6000 Assay Kit on a Bioanalyzer 2100 system (Agilent Technologies). mRNA was purified from total RNA using poly-T oligo-attached magnetic beads, fragmented and then used for first strand cDNA synthesis with random hexamer primers and M-MuLV Reverse Transcriptase. This was followed by RNA degradation with RNase H. Second-strand cDNA synthesis was performed using DNA Polymerase I and dNTPs to convert the overhangs into blunt ends, followed by adenylation and adaptor ligation. Selected cDNA fragments of 370–420 bp were purified using AMPure XP beads, amplified by PCR and purified again. Libraries were quantified using a Qubit 2.0 Fluorometer and quality-checked with an Agilent 2100 bioanalyzer before sequencing on the Illumina NovaSeq 6000 platform to generate 150 bp paired-end reads. Clean reads were mapped to the reference genome using the HISAT2 software. Gene ontology (GO) and Kyoto Encyclopedia of Genes and Genomes (KEGG) enrichment analysis of the differentially expressed genes (DEGs) was performed using the ClusterProfiler R package (3.8.1). The GSEA software (v4.3.2) was employed to identify gene expression patterns that are linked to particular biological functions or pathways.

2.12 | Non-targeted metabolomics analysis

A non-targeted metabolomic analysis was conducted using LC–MS/MS by Novogene Co., Ltd., Beijing, employing a Vanquish UHPLC system coupled with a Q Exactive HF mass spectrometer (Thermo Fisher, Germany). AML12 cells were cultured to 80% confluence, harvested, washed with PBS and resuspended in prechilled 80% methanol. Metabolites were extracted through liquid nitrogen freezing, thawing, vortexing, sonication and centrifugation at 15 000 g for 20 min at 4°C. The supernatant was lyophilized and dissolved in 10% methanol before injection into the LC–MS system. The analysis utilized a Hypersil Gold C18 column (100 × 2.1 mm, 1.9 μm) with a 12-min solvent gradient in both positive and negative ion modes. Raw data were processed using Compound Discoverer 3.1, including peak alignment, deconvolution and normalization to total spectral intensity, with compounds showing a coefficient of variation (CV) > 30% in quality control samples excluded. Metabolites were annotated using mzCloud, mzVault and MassList databases, and differential metabolites were identified based on thresholds of VIP >1, p-value <0.05 and fold change ≥2 or ≤0.5. Heatmaps were generated with the pheatmap package in R software.

2.13 | Statistical analyses

All experiments were conducted in triplicate to ensure reliability. Statistical analyses were performed using the SPSS software (version 21.0; IBM, Armonk, NY, USA). Data are expressed as the mean ± SEM. An independent t test was used to compare two samples. Statistical significance was defined as $p < 0.05$.

3 | RESULTS

3.1 | *Rap1b* expression is negatively associated with obesity in humans and mice

To investigate the association between *Rap1b* expression levels and obesity and related diseases, we analysed *Rap1b* mRNA expression in human liver samples obtained from morbidly obese patients and normal controls sourced from the published GEO database (GSE61260).[21] *Rap1b* mRNA expression was significantly lower in patients with obesity than in healthy controls (Figure 1A). Additionally, we examined another dataset (GSE126848), which included liver biopsy samples from normal-weight individuals (normal, $n = 14$), obese individuals ($n = 12$), patients with simple steatosis (NAFL, $n = 15$) and patients with nonalcoholic steatohepatitis (NASH, $n = 16$).[22] In this dataset, *Rap1b* mRNA expression was significantly lower in both NAFL and NASH (Figure 1B). Regardless of the presence of type 2 diabetes mellitus, *Rap1b* expression was significantly reduced in obese individuals from the GSE15653 dataset (Figure 1C).[23] Subsequently, we analysed liver tissues from male mice fed either a standard diet (SD) or HFD. qRT-PCR (Figure 1D) and WB (Figure 1E) analyses showed a significant decrease in RAP1B expression in HFD-induced obese mice. Lower expression of *Rap1b* mRNA (Figure 1F) and RAP1B protein (Figure 1G) was observed in DB/DB mice than in the controls. To mimic these conditions in vitro, we treated AML12 hepatocyte cells with 200-μM palmitic acid (PA), which
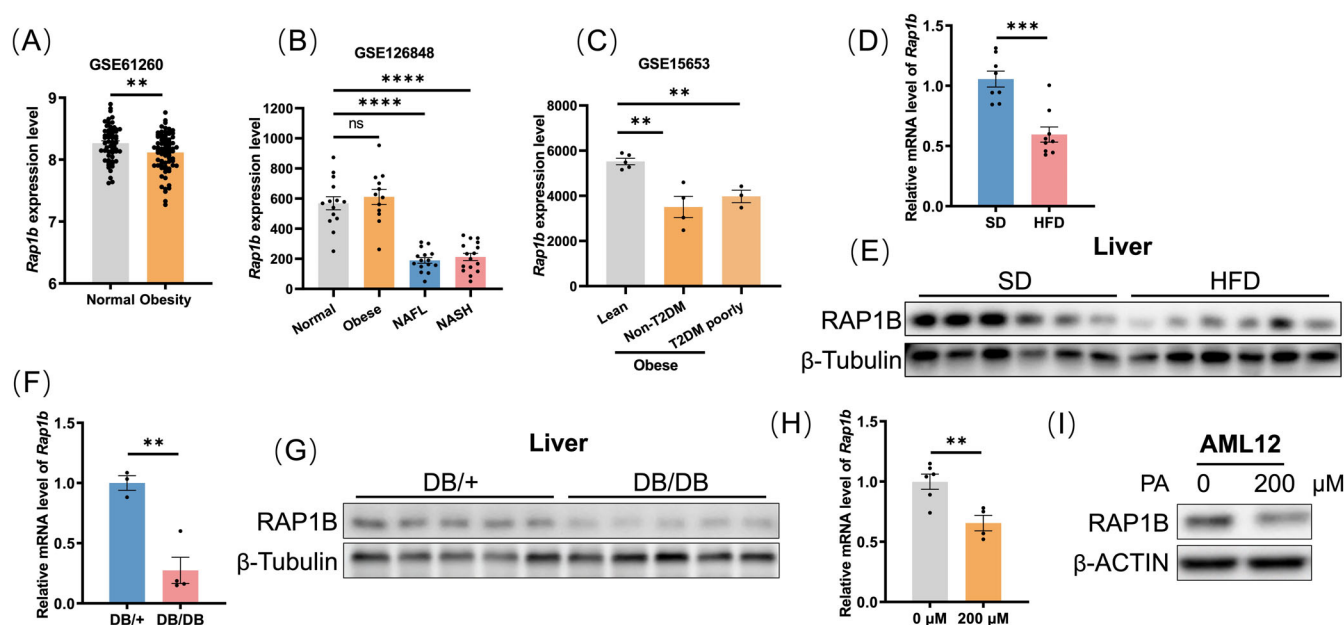
FIGURE 1 *Rap1b* expression is negatively associated with obesity in humans and mice. (A) Comparative analysis of *Rap1b* mRNA levels in liver samples from morbidly obese patients and normal controls, based on data from the GEO database (GSE61260). (B) *Rap1b* mRNA levels in liver biopsies from normal-weight individuals (Normal, $n = 14$), obese individuals ($n = 12$), patients with simple steatosis (NAFL, $n = 15$) and nonalcoholic steatohepatitis patients (NASH, $n = 16$), sourced from GSE126848. (C) Comparison of *Rap1b* mRNA levels in liver samples from lean controls undergoing elective cholecystectomy ($n = 5$) and obese patients undergoing gastric bypass surgery, both non-T2DM and T2DM ($n = 13$), sourced from GSE15653. (D, E) *Rap1b* mRNA (D) and protein (E) levels in liver tissues from C57BL/6 mice fed a standard diet (SD) or high-fat diet (HFD). (F, G) Analysis of *Rap1b* mRNA (F) and protein (G) levels in liver tissues from DB/m and DB/DB male mice. (H, I) Quantification of *Rap1b* mRNA (H) and RAP1B protein (I) levels in AML12 cells treated with palmitic acid (PA) compared with untreated controls. Data are presented as the mean ± SEM, derived from at least three independent experiments. Significant differences are indicated as *$p < 0.05$, **$p < 0.01$, ***$p < 0.001$, ****$p < 0.0001$; ns, not significant.

led to decreased *Rap1b* mRNA (Figure 1H) and RAP1B protein levels (Figure 1I). Overall, our comprehensive analysis suggests a significant reduction in RAP1B expression in the liver tissues and cells of obese mice compared with that in their normal-weight counterparts, indicating a potential mechanistic role of *Rap1b* in the pathophysiology of obesity and related metabolic disorders.
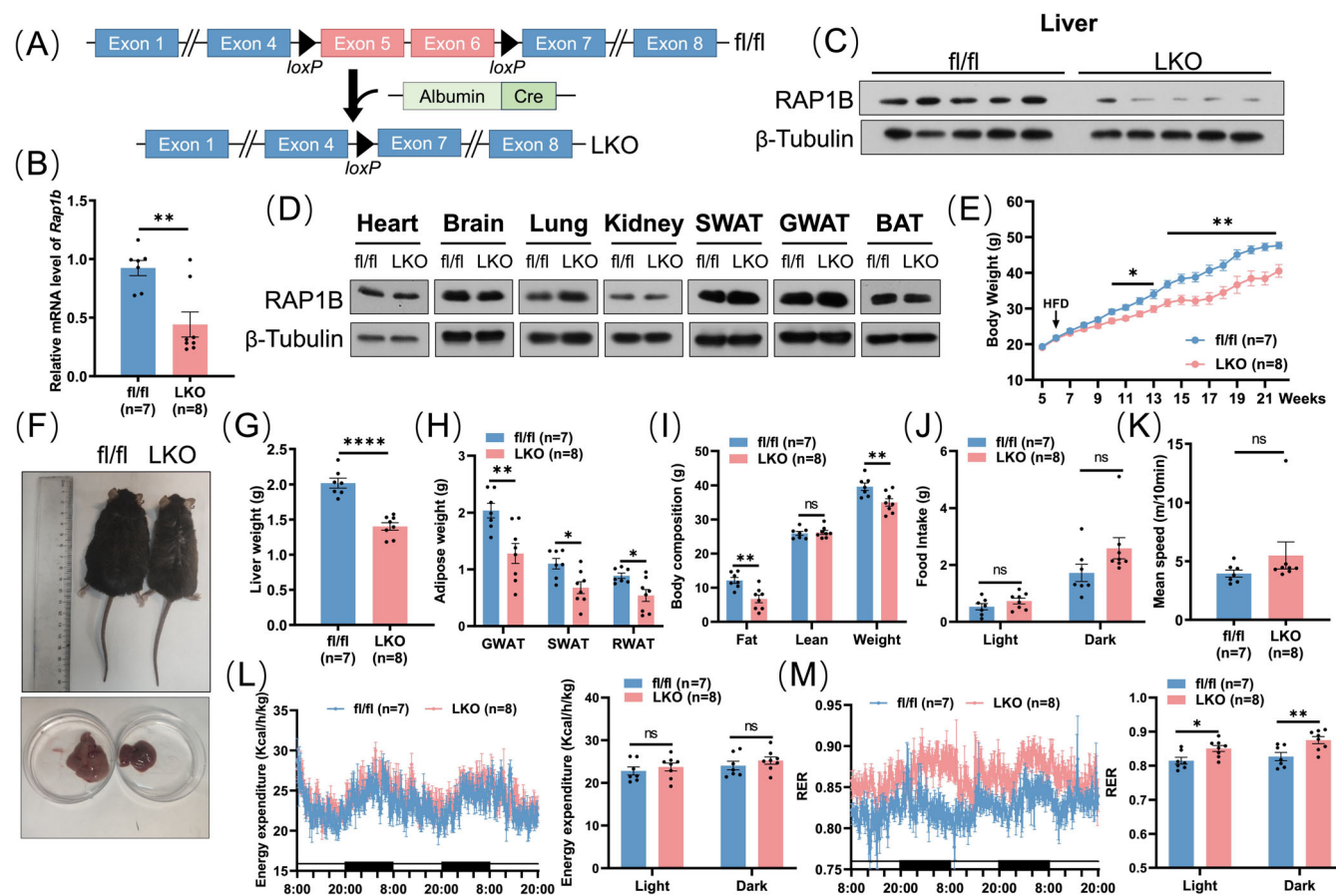
3.2 | Liver-specific *Rap1b* knockout (LKO) alleviates HFD-induced obesity in mice

Owing to the close link between liver and whole-body metabolism, we established a liver-specific *Rap1b*-knockout mouse model using the C57BL/6 strain (Figure 2A). Liver tissues from the LKO mice showed a significant decrease in *Rap1b* mRNA and RAP1B protein levels, as evidenced by qRT-PCR (Figure 2B) and WB (Figure 2C). In contrast, RAP1B protein levels remained unchanged in non-liver tissues, including the heart, brain, lungs, kidneys and adipose tissues (Figure 2D), confirming the specificity of the knockout. To explore the link between *Rap1b* and obesity-related metabolic disorders, we fed male mice aged 6–8 weeks a HFD for at least 18 weeks. After the seventh week, the LKO mice consistently displayed lower body weights (Figure 2E) and smaller sizes (Figure 2F) than the fl/fl mice. Remarkably, the LKO mice also showed significantly lower liver weights (Figure 2G) and reduced fat pad sizes (Figure 2H) than the

fl/fl controls. An analysis using an echoMRI body composition analyser revealed a significant reduction in fat mass in the LKO mice, whereas there was no significant change in lean mass (Figure 2I). To explore the mechanism by which hepatic RAP1B deletion protects mice from HFD-induced obesity, we observed that the LKO mice showed no significant differences in daily food intake (Figure 2J) or activity levels (Figure 2K) compared with the fl/fl mice. However, under HFD conditions, the LKO mice demonstrated unchanged EE (Figure 2L) and elevated respiratory exchange ratios (RERs) (Figure 2M). These findings confirm that hepatic RAP1B deletion significantly reduced body and liver weights, as well as fat mass, in HFD-fed mice relative to the controls, suggesting that RAP1B is a promising therapeutic target for managing obesity and related metabolic disorders.

3.3 | Hepatic deficiency of *Rap1b* ameliorates HFD-induced insulin resistance

To elucidate the metabolic profiles of the LKO mice, which showed lower body weights and higher EE, we performed a GTT and ITT. The GTT revealed enhanced glucose tolerance in the LKO mice, which was characterized by lower postprandial glucose levels (Figure 3A). The ITT results showed improved insulin sensitivity, as demonstrated by a more significant reduction in blood glucose after insulin

FIGURE 2 Liver-specific *Rap1b* knockout alleviates HFD-induced obesity in mice. (A) Strategy used to generate liver-specific *Rap1b* knockout mice. (B) mRNA levels of *Rap1b* in liver samples from fl/fl and LKO mice, $n = 7–8$ per group. (C) Western blot analysis demonstrating RAP1B protein expression in liver tissues from the studied mice, $n = 5$. (D) Western blot analysis demonstrating RAP1B protein expression in non-liver tissues from the studied mice. (E) Weekly tracking of body weight in fl/fl and LKO male mice fed a HFD at 6 weeks of age, $n = 7–8$ per group. (F) Comparative gross morphology of fl/fl and LKO mice body size and liver. (G) Liver weight of HFD-fed fl/fl and LKO male mice, $n = 7–8$ per group. (H) Weights of GWAT, SWAT and RWAT in fl/fl and LKO male mice, $n = 7–8$ per group. (I) Body composition analysis of fl/fl and LKO male mice, $n = 7–8$ per group. (J) Daily food intake of fl/fl and LKO male mice during light and dark cycles, $n = 7–8$ per group. (K) Locomotor activity assessment in fl/fl and LKO male mice, $n = 7–8$ per group. (L) Energy expenditure curves and average energy expenditure during light and dark in fl/fl and LKO male mice with lean mass as a covariate for normalization, $n = 7–8$ per group. (M) RER curves and average RER during light and dark phases were calculated by dividing carbon dioxide output (VCO_2) by oxygen uptake (VO_2), $n = 7–8$ per group. Data are presented as the mean ± SEM, derived from at least three independent experiments. Significant differences are indicated as *$p < 0.05$, **$p < 0.01$, ***$p < 0.001$, ****$p < 0.0001$; ns, not significant.

administration than in the fl/fl mice (Figure 3B). A serum insulin analysis showed no notable changes (Figure 3C), indicating that hepatic RAP1B did not influence insulin secretion. The LKO mice exhibited unchanged levels of serum TG and NEFA levels (Figure 3D,E). Stable TG and NEFA levels may result from compensatory metabolic processes in adipose tissue or other peripheral tissues that maintain the overall lipid balance.[24] Our findings indicate that hepatic RAP1B deficiency enhances insulin sensitivity .

3.4 | Hepatic RAP1B deficiency reduces liver lipid accumulation

To assess the impact of RAP1B knockout on the liver, we performed H&E staining to examine liver morphology and identify any

histological changes. The results of H&E staining revealed a reduction in lipid vacuoles within the liver tissues of the LKO mice (Figure 4A), and Oil Red O staining confirmed the presence of fewer lipid droplets (Figure 4B). Notably, the levels of TG (Figure 4C) and glycerol (Figure 4D) were significantly lowered in the livers of LKO mice, hinting at perturbations in hepatic lipid metabolism. Further gene expression analyses related to lipogenesis and lipolysis revealed an increased expression of key lipolysis-related genes, including *Lpl*, *Cpt1a*, *Cpt2* and *Atgl* in the LKO mice (Figure 4E). Notably, CPT1A and ATGL, which are crucial for fatty acid oxidation and TG catabolism, were significantly upregulated, indicating enhanced lipolysis. Conversely, the expression of the lipogenesis-associated protein FASN was markedly suppressed (Figure 4F). Subsequently, we established a RAP1B KD cell model, in which WB (Figure 4G) and qRT-PCR (Figure 4H) analyses confirmed significant reductions in *Rap1b* mRNA and RAP1B
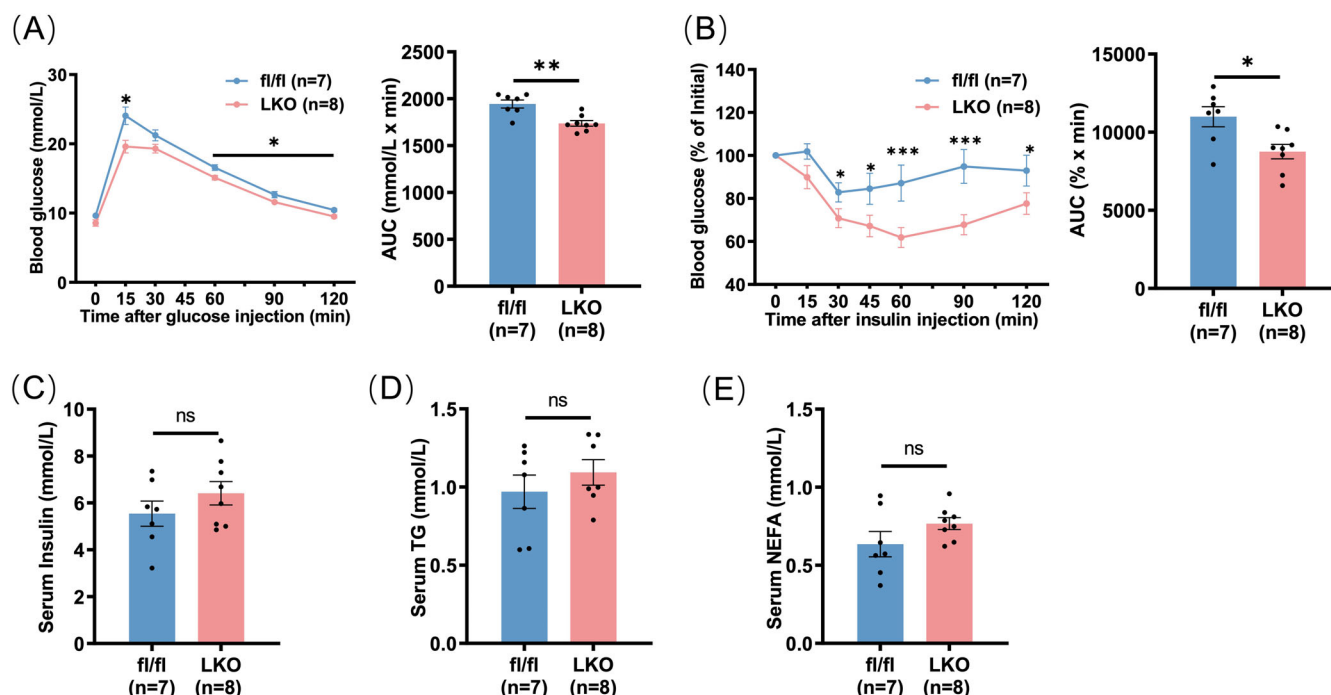
FIGURE 3 Hepatic deficiency of *Rap1b* ameliorates HFD-induced insulin resistance. (A) GTT was performed at week 19 in fl/fl and LKO mice with a subsequent area under the curve (AUC) analysis, $n = 7-8$ per group. (B) ITT was performed at week 20 in fl/fl and LKO mice with an AUC quantification to evaluate insulin sensitivity. (C) Serum insulin concentrations in HFD-fed fl/fl and LKO male mice, $n = 7-8$ per group. (D, E) TG (G) and NEFA (E) levels in serum of fl/fl and LKO mice fed HFD, $n = 7-8$ per group. Data are presented as the mean ± SEM, derived from at least three independent experiments. Significant differences are indicated as *$p < 0.05$, **$p < 0.01$, ***$p < 0.001$, ****$p < 0.0001$; ns, not significant.

protein levels. Consistently, Oil Red O staining (Figure 4I) and TG measurements (Figure 4J) indicated reduced lipid accumulation in RAP1B KD cells compared with Ctrl cells. Furthermore, non-targeted metabolomics analysis unveiled a notable decrease in fatty acid diversity within KD cells (Figure 4K). Gene Ontology Biological Process (GO_BP) pathway analyses of the transcriptomic data from AML12 Ctrl and KD cells revealed substantial alterations in pathways governing fatty acid and lipid metabolism (Figure 4L). Taken together, the observed decline in lipid accumulation in both the liver tissues of LKO mice and RAP1B KD cells underscores the pivotal role of RAP1B in maintaining lipid homeostasis and highlights the intensified lipolysis that occurs in its absence.

3.5 | Hepatic inflammation and oxidative stress diminish and correlate with hepatic RAP1B deficiency

To investigate the underlying mechanisms through which RAP1B impacts lipid metabolism, we conducted an in-depth GSEA analysis on RAP1B KD cells, identifying significant changes in inflammation-related pathways, including TNF, IL-17, MAPK and NF-κB signalling pathways (Figure 5A). Inflammation often triggers the production of reactive oxygen species (ROS), which in turn induces oxidative stress and lipid peroxidation. To assess these processes, we measured cellular MDA (Figure 5B) and catalase activity (Figure 5C), both of which showed significant reductions in KD cells compared with Ctrl cells,

suggesting a decrease in oxidative stress levels and lipid peroxidation, likely as a consequence of reduced inflammatory signalling. Furthermore, when compared with fl/fl mice, the transcriptional levels of pro-inflammatory factors such as *Tnf-α* and *Ccl2*, as well as the protein levels of CCL2, IL-6 and IL-1β, were markedly decreased in the liver tissues of LKO mice (Figure 5D,E). Immunohistochemical analysis of F4/80, a macrophage marker, showed reduced expression in the liver of LKO mice (Figure 5F,G), indicating diminished inflammation. Additionally, both KD cell models (Figure 5H) and LKO mouse livers (Figure 5I) exhibited significant reductions in phosphorylated NF-κB (p-NF-κB) and phosphorylated MAPK (p-MAPK), critical mediators of inflammatory signalling. Collectively, these findings suggest that RAP1B deficiency leads to decreased NF-κB and MAPK activation, which in turn results in diminished inflammatory signalling and oxidative stress, thereby mitigating metabolic disturbances.

3.6 | Hepatic RAP1B OE increases body weight and aggravates glucose metabolism dysfunction

Building on the findings from the LKO mice, which demonstrated the protective effects of hepatic RAP1B deletion against obesity and metabolic dysfunction, we further investigated the impact of hepatic RAP1B OE (Figure 6A). We confirmed the successful OE of RAP1B in the liver through qRT-PCR (Figure 6B) and WB analysis (Figure 6C,D), with no detectable RAP1B expression increase in other tissues.
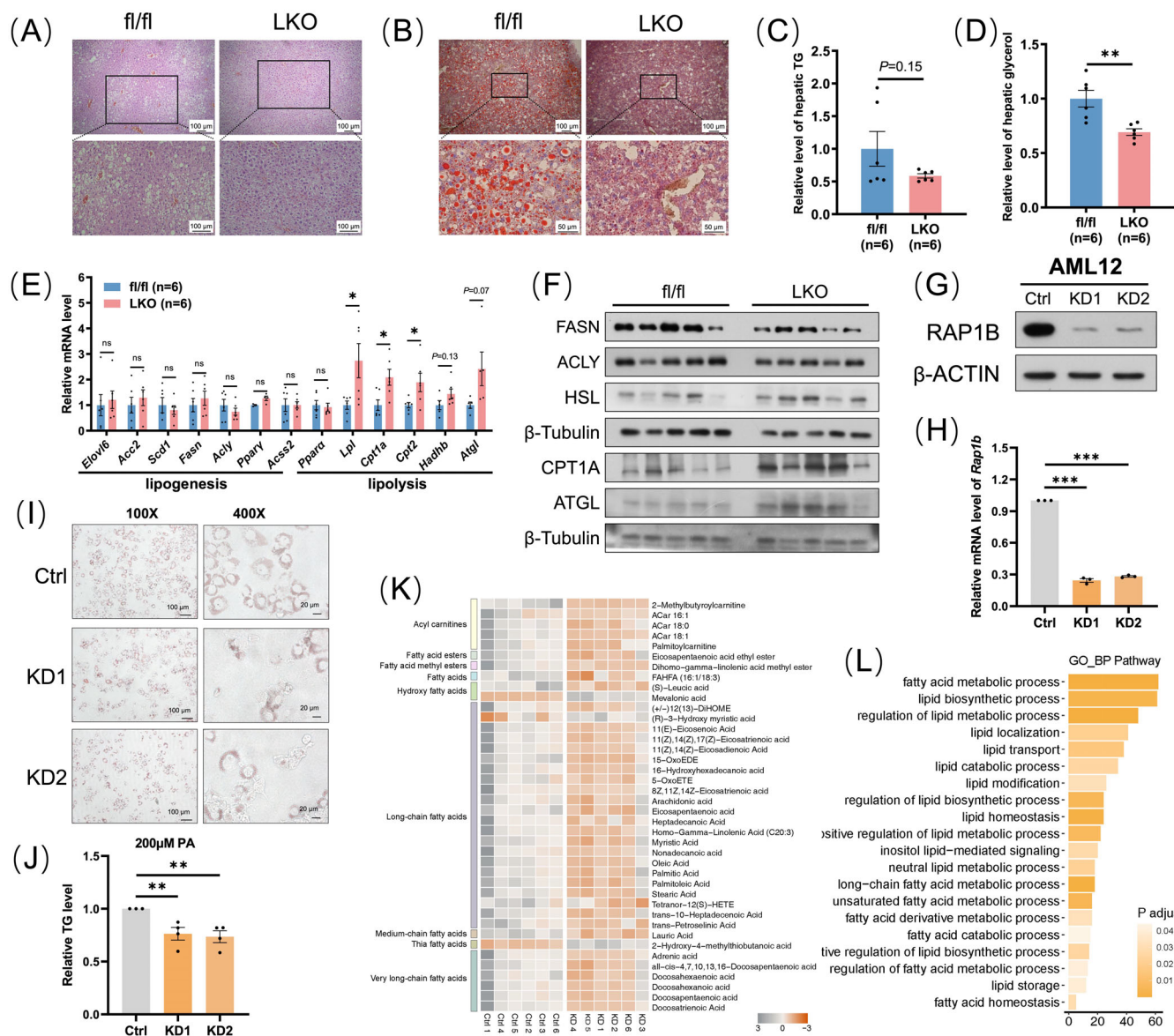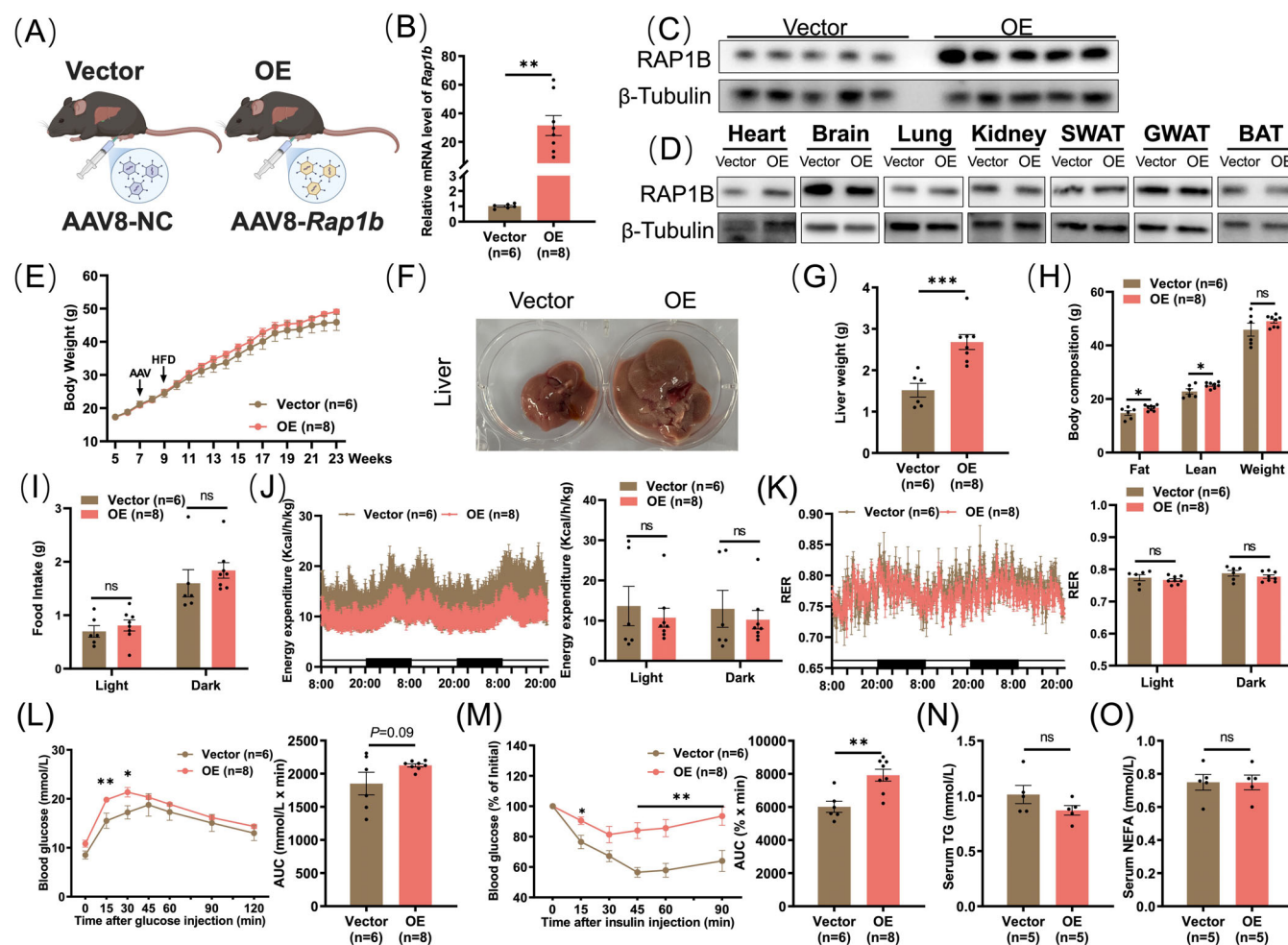
FIGURE 4 Hepatic RAP1B deficiency reduces liver lipid accumulation. (A, B) H&E (A) and Oil Red O (B) staining of liver sections from fl/fl and LKO mice fed a HFD, displaying lipid distribution. (C, D) Quantification of TG (C) and glycerol (D) in liver tissues of fl/fl and LKO mice ($n = 6$). (E) mRNA levels of genes related to lipogenesis and lipolysis in liver tissues of fl/fl and LKO mice, $n = 6$. (F) Western blot analysis of proteins involved in lipogenesis and lipolysis in liver tissues from HFD-fed fl/fl and LKO mice, $n = 5$. (G) Western blot analysis of RAP1B proteins in AML12 Ctrl and KD cells. (H) Quantification of *Rap1b* mRNA expression levels in AML12 Ctrl and KD cells. (I) Oil Red O staining in AML12 Ctrl and KD cells treated with 200-μM PA, illustrating lipid droplets at 100x and 400x magnification. (J) TG levels in AML12 Ctrl and KD cells post PA treatment. (K) Heatmap of lipid-related species identified by untargeted metabolomics in AML12 Ctrl and KD cells, $n = 6$. (L) Gene Ontology Biological Process (GO_BP) analysis for differentially expressed genes in AML12 Ctrl and KD cells. Data are presented as the mean ± SEM, derived from at least three independent experiments. Significant differences are indicated as *$p < 0.05$, **$p < 0.01$, ***$p < 0.001$; ns, not significant.

Although there was no significant difference in body weight (Figure 6E), the liver size and weight of OE mice showed a significant increase compared with those of the Vector mice (Figure 6F,G). The body composition analyser revealed a significant increase in fat and lean mass in the OE mice (Figure 6H). However, there were no significant differences in food intake (Figure 6I), EE (Figure 6J) or RER (Figure 6K). Metabolic assessments further revealed impaired glucose tolerance and reduced insulin sensitivity in OE mice, as indicated by

GTT and ITT results, which showed an upgliding trend in blood glucose levels and diminished responsiveness to insulin (Figure 6L,M). Serum lipid analyses in OE mice revealed unchanged levels of TG (Figure 6N) and NEFA (Figure 6O). These findings indicate that hepatic RAP1B OE leads to increased body weight and impaired glucose metabolism, promoting localized liver enlargement without affecting overall energy balance or dietary intake, highlighting a distinct metabolic impact compared with hepatic RAP1B deletion.

FIGURE 5 Hepatic inflammation and oxidative stress diminish and correlate with hepatic RAP1B deficiency. (A) Gene Set Enrichment Analysis (GSEA) identifying significantly enriched pathways in AML12 Ctrl and KD cells. (B) Malondialdehyde (MDA) content in AML12 Ctrl and KD cells. (C) Catalase activity measurements in AML12 Ctrl and KD cells. (D) Quantification of mRNA expression levels of pro-inflammatory factors in liver tissues from fl/fl and LKO mice, $n = 3$ per group. (E) Western blot analysis of proteins involved in inflammatory factors in liver tissues from HFD-fed fl/fl and LKO mice, $n = 5$. (F, G) Immunohistochemical staining for F4/80 in liver tissues from HFD-fed fl/fl and LKO mice (F), with quantitative analysis of macrophage infiltration (G), $n = 3$. (H, I) Western blot analysis of phosphorylated and total NF-κB (p65) and MAPK (p38) proteins in AML12 cells (H) and liver tissues of mice (I). (J) Graphical abstract illustrating the regulation of high-fat diet-induced obesity and liver inflammation by RAP1B in mice, created with BioRender.com. Data are presented as the mean ± SEM, derived from at least three independent experiments. Significant differences are indicated as *$p < 0.05$, **$p < 0.01$; ns, not significant.

3.7 | Hepatic RAP1B increases liver lipid accumulation and enhances hepatic inflammation

Furthermore, hepatic lipid accumulation was significantly increased in OE mice, with more pronounced lipid vacuoles and droplets evident in H&E and Oil Red O staining (Figure 7A,B), accompanied by elevated hepatic TG, NEFA and glycerol (Figure 7C–E). At the molecular level, although the mRNA levels of both lipolysis and lipogenesis-related genes were increased in OE mice (Figure 7F), the WB analysis revealed reduced expression of lipolysis-related proteins, including CPT1A and ATGL, alongside increased expression of the lipogenesis-associated protein FASN and ACLY (Figure 7G), in stark contrast to the enhanced lipolysis observed in LKO mice. Conversely, when compared with Vector mice, in the liver tissues of OE mice, a significant upregulation of Tnf-α, Ccl2 and Ifn-γ was detected at the transcriptional level (Figure 7H), accompanied by an increase in the protein expression of CCL2, IL-6 and IL-1β, which together strongly suggest a shift toward a pro-inflammatory environment (Figure 7I). Additionally, immunohistochemical staining of F4/80 further confirmed heightened expression in the livers of OE mice compared with that of Vector mice

(Figure 7J,K), indicating amplified inflammation within the OE mice's livers. In the OE mouse liver models, we observed a notable increase in p-NF-κB and p-MAPK levels (Figure 7L), indicating the activation of these critical inflammatory signalling pathways. Collectively, these findings demonstrate that hepatic RAP1B OE exacerbates lipid accumulation and hepatic inflammation, underscoring its role in driving metabolic disorders in contrast to the protective effects of hepatic RAP1B deletion.

4 | DISCUSSION

Obesity significantly increases the risk of various metabolic diseases, such as diabetes and cardiovascular disorders, which are primarily driven by an imbalance between energy intake and expenditure.[25] The liver plays a central role in maintaining systemic energy homeostasis, making it a key organ for regulating metabolic health.[26] While existing literature predominantly examined RAP1B's involvement in tumour development, cell adhesion and proliferation,[27] emerging studies indicate its regulatory function in glucose and lipid
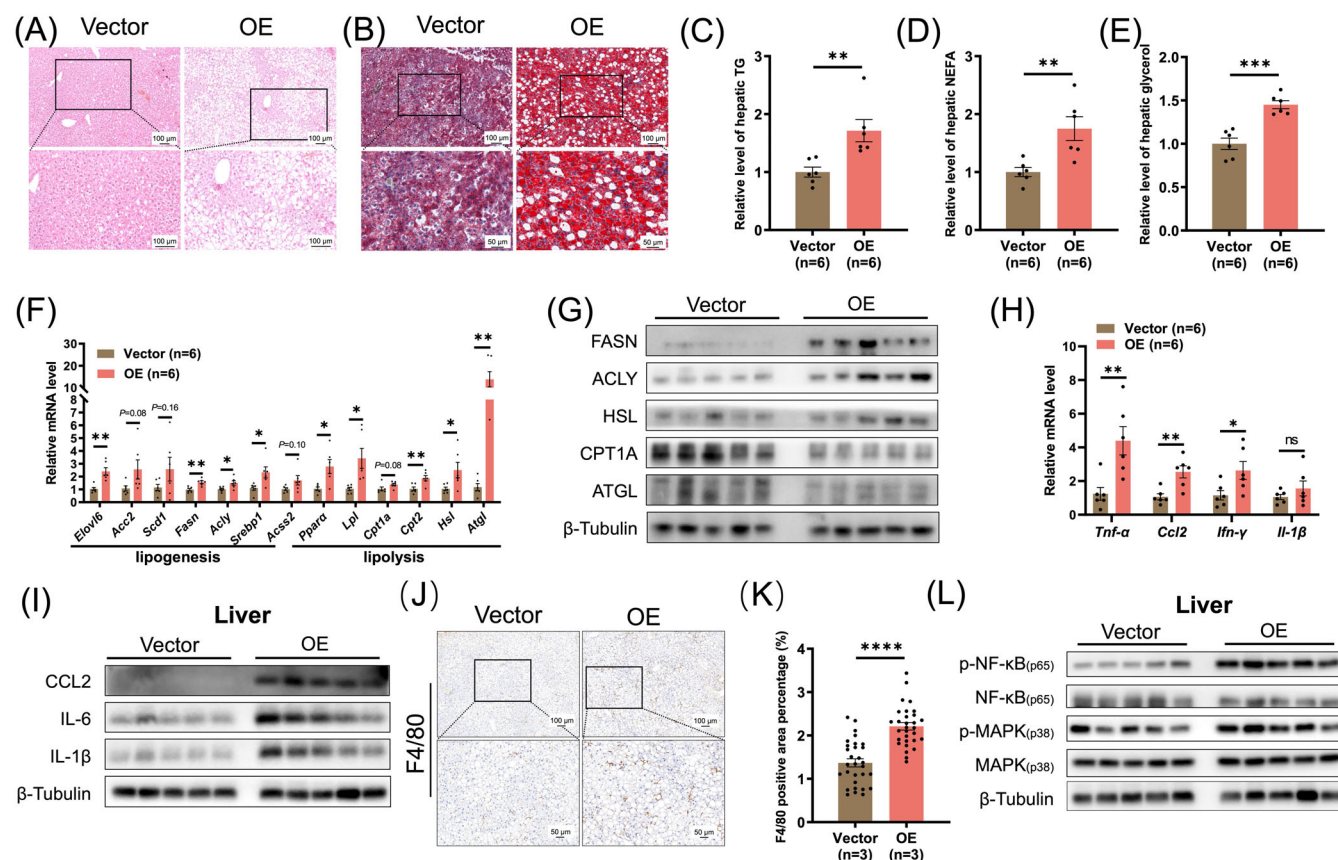
FIGURE 6 Hepatic RAP1B overexpression (OE) increases body weight and aggravates glucose metabolism dysfunction. (A) The strategy used to obtain liver-specific RAP1B OE mice. Created with BioRender.com. (B) mRNA levels of *Rap1b* in liver samples from Vector and OE mice. (C) Western blot analysis demonstrating RAP1B protein expression in liver tissues from the studied mice, $n = 5$. (D) Western blot analysis demonstrating RAP1B protein expression in non-liver tissues from the studied mice. (E) Weekly tracking of body weight in Vector and OE male mice fed. (F) Comparative gross morphology of liver in Vector and OE mice. (G) Liver weight of HFD-fed Vector and OE male mice. (H) Body composition analysis of Vector and OE male mice. (I) Daily food intake of Vector and OE male mice during light and dark cycles. (J) Energy expenditure curves and average energy expenditure during light and dark in Vector and OE male mice with lean mass as a covariate for normalization. (K) RER curves and average RER during light and dark phases were calculated by dividing carbon dioxide output (VCO_2) by oxygen uptake (VO_2). (L) GTT was performed at week 20 in Vector and OE mice with a subsequent area under the curve (AUC) analysis. (M) ITT was performed at week 21 in Vector and OE mice with an AUC quantification to evaluate insulin sensitivity. $n = 6$–8 per group. (N, O) TG (N), NEFA (O) levels in serum of Vector and OE mice fed HFD, $n = 5$ per group. Data are presented as the mean ± SEM, derived from at least three independent experiments. Significant differences are indicated as $**p < 0.01$, $***p < 0.001$; ns, not significant.

metabolism.[28,29] Notably, upregulation of *Rap1b* mRNA in renal tubular cells of diabetic nephropathy mice correlates with elevated blood glucose levels, suggesting a role in glucose metabolism.[18] However, the specific functions of RAP1B in liver tissue and its impact on lipid metabolism have remained unclear, creating a critical gap in our understanding of its broader metabolic functions.

Our study aimed to address the gap in knowledge regarding the role of RAP1B in liver lipid metabolism, with a particular focus on its involvement in metabolic disorders induced by obesity. Preliminary data from human and murine studies show that RAP1B expression is downregulated in the liver under conditions of obesity and metabolic

disturbances.[21–23] Consistent with these observations, we found reduced RAP1B expression in diet-induced obese mice, DB/DB mice and AML12 cells treated with palmitic acid, reinforcing the hypothesis that RAP1B plays a critical role in regulating hepatic metabolism under metabolic stress.

In our study, we used LKO mice to investigate the consequences of RAP1B deficiency on hepatic lipid metabolism. The choice of a tissue-specific knockout model was crucial, as whole-body knockout of RAP1B has been shown to result in potential 40% embryonic lethality,[30] thus limiting the ability to study its effects in mature organisms. This is consistent with other recent studies that have utilized

FIGURE 7 Hepatic RAP1B increases liver lipid accumulation and enhances hepatic inflammation. (A, B) H&E (A) and Oil Red O (B) staining of liver sections from Vector and overexpression (OE) mice fed HFD. (C–E) Relative levels of TG (C), NEFA (D) and glycerol (E) in liver tissues of Vector and OE mice ($n = 6$). (F) mRNA levels of genes related to lipogenesis and lipolysis in liver tissues of Vector and OE mice, $n = 6$. (G) Western blot analysis of proteins involved in lipogenesis and lipolysis in liver tissues from HFD-fed Vector and OE mice, $n = 5$. (H) Quantification of mRNA expression levels of pro-inflammatory factors in liver tissues from Vector and OE mice, $n = 6$ per group. (I) Western blot analysis of proteins involved in inflammatory factors in liver tissues from HFD-fed Vector and OE mice, $n = 5$. (J, K) Immunohistochemical staining for F4/80 in liver tissues from HFD-fed Vector and OE mice (J), with quantitative analysis of macrophage infiltration (K), $n = 3$. (L) Western blot analysis of phosphorylated and total NF-κB (p65) and MAPK (p38) proteins in and liver tissues of mice. Data are presented as the mean ± SEM, derived from at least three independent experiments. Significant differences are indicated as *$p < 0.05$, **$p < 0.01$, ***$p < 0.001$; ns, not significant.

tissue-specific knockouts to explore the metabolic roles of genes in a more controlled manner.[31,32] By avoiding the lethal effects of full-body RAP1B knockout, we were able to assess the in vivo effects of RAP1B deficiency specifically in the liver. Notably, LKO mice exhibited significantly reduced body weight, smaller fat pads and lower liver weights compared with the control group, indicating a protective role against diet-induced obesity. These results support the idea that hepatic RAP1B signalling contributes significantly to the regulation of energy homeostasis, a concept that aligns with recent findings highlighting the liver's central role in obesity-related metabolic disorders.[33] In contrast to the protective effects observed in the LKO mice, the RAP1B OE mice exhibited increased liver weight and lipid accumulation, along with worsened insulin resistance, highlighting the opposing effects of RAP1B on lipid metabolism. These results are not consistent with studies that RAP1B has been shown RAP1B to inhibit autophagy and apoptosis under high glucose conditions by stabilizing the Bcl-2/Bax complex, indicating a protective role of RAP1B in the

kidneys.[17,18] However, RAP1B appears to have a different function in the central nervous system, potentially contributing to the reduction of obesity.[29] These findings underscore the necessity for further investigation into the distinct mechanisms and pathways through which RAP1B may exert its effects across different organs.

Lipid accumulation in the liver is a critical feature of obesity and associated metabolic disorders, including hepatic steatosis and insulin resistance.[34,35] In our LKO mice, we observed significantly reduced hepatic TG and glycerol levels. This reduction in hepatic lipid accumulation was not solely attributed to decreased levels of the lipogenic enzyme FASN, but rather to an increase in lipid catabolism, as shown by the upregulation of genes involved in fatty acid oxidation (*Cpt1a*, *Cpt2*, *Lpl*, and *Atgl*). These results were supported by RAP1B knockdown (KD) cells, where Oil Red O staining and TG quantification confirmed a similar reduction in lipid accumulation. This shift toward more active lipolysis and fatty acid catabolism played a significant role in reducing hepatic lipid content. The increased hepatic TG, NEFA and

glycerol levels were observed in OE mice, along with the heightened lipid accumulation evident in Oil Red O and H&E staining. This is consistent with studies demonstrating that the upregulation of fatty acid oxidation genes can reduce lipid accumulation and protect against obesity-related liver dysfunction, such as XBP1, which played a key role in promoting fatty acid oxidation and reducing hepatic lipid accumulation.[36,37]

Additionally, chronic inflammation and oxidative stress play pivotal roles in the pathogenesis of obesity-related metabolic disorders, particularly in the liver.[38,39] Our transcriptomic analysis of RAP1B KD cells further identified differentially expressed genes (DEGs) associated with inflammation, particularly involving the NF-κB and MAPK pathway, which are well-known mediators of inflammation in metabolic diseases.[40–43] In contrast, like the anti-inflammatory effects observed in FGL2 studies,[44] RAP1B deficiency in the liver resulted in reduced inflammation and oxidative stress, as evidenced by lower levels of pro-inflammatory cytokines (*Tnf-α* and *Ccl2*) and decreased macrophage infiltration. OE mice were likely to exhibit a pro-inflammatory hepatic environment, as inferred from the contrasting phenotypes. These findings align with studies suggesting that inflammation and oxidative stress contribute to hepatic lipid accumulation and insulin resistance.[45–48] Previous research has also explored the role of RAP1B as an upstream regulator of NF-κB in bone marrow-derived macrophages.[49] This discrepancy suggests the need for further investigation into the interactions between hepatocytes and macrophages within the liver microenvironment. Based on the WB results and the role of MAPK(p38) and NF-κB in cellular inflammation and metabolic regulation,[50,51] we can hypothesize that RAP1B may modulate the MAPK(p38) pathway, potentially influencing its activation. This modulation could affect the downstream activation of NF-κB, impacting the expression of inflammatory cytokines and adipokines, which are critical in metabolic regulation. Currently, no specific pharmacological agents targeting RAP1B are available, and further research is needed to develop selective agents and assess their safety profiles. In our study, we utilized an AAV-mediated OE approach to modulate RAP1B in the liver, which revealed significant effects on obesity-related metabolic parameters, although the OE model led to increased obesity. This highlights RAP1B as a potential therapeutic target and supports the use of AAV-based gene therapy in preclinical models. Additionally, gene silencing techniques, such as AAV-mediated shRNA, could be valuable for evaluating RAP1B inhibition in obesity and metabolic disorders. However, the efficacy and safety of these strategies must be thoroughly evaluated before clinical application. Importantly, our results further demonstrate that RAP1B may modulate inflammation and oxidative stress, which could offer insights into new therapeutic strategies for treating obesity and metabolic syndrome.

Despite the observed decrease in RAP1B expression in the liver tissues of obese individuals, our LKO mice exhibited an enhanced overall metabolic profile. This paradoxical observation could be attributed to compensatory mechanisms that are activated in the absence of RAP1B, leading to improved metabolic functions.[52] While our findings highlight the role of RAP1B in liver metabolism, further investigations are needed to explore potential crosstalk between the liver and adipose tissue in regulating lipid metabolism.[53] Given that adipose tissue also plays a critical role in lipid homeostasis, understanding the interaction between the liver and adipose tissue may provide a more comprehensive view of the metabolic effects of RAP1B.[32,54] Moreover, although our study suggests that hepatic RAP1B deficiency reduces inflammation and oxidative stress, the specific molecular mechanisms by which RAP1B modulates these processes require further investigation.

In conclusion, this study reveals the critical role of RAP1B in hepatic lipid metabolism and its impact on metabolic health. Our results suggest that hepatic RAP1B deficiency enhances lipolysis, reduces hepatic lipid accumulation and improves the metabolic profile, whereas RAP1B OE exacerbates metabolic dysregulation. These findings underscore the potential of RAP1B as a therapeutic target for obesity, hepatic steatosis and related metabolic disorders.

AUTHOR CONTRIBUTIONS

Qiongya Zhao and Jianxin Lyu conceived and designed the experiments. Yinxu Fu acquired and analysed data and drafted the manuscript. Yinxu Fu, Pingyi Hu, Yanyang Hu, Yu Fang, Yaping Zhou, Yu Shi and Kaiqiang Yang performed the experiments and data collection. Ting Fu, Weijia Li, Gritskevitch Evgeniy Rostislavovich and Liqin Jin contributed to the data discussion. Liqin Jin, Jianxin Lyu and Qiongya Zhao are the guarantors of this work and take responsibility for the accuracy of the data analysis. Qiongya Zhao reviewed and edited the manuscript. All authors have approved the final version to be published.

ACKNOWLEDGEMENTS

FUNDING INFORMATION

CONFLICT OF INTEREST STATEMENT

The authors declare that they have no known competing financial interests or personal relationships that could have appeared to influence the work reported in this paper.

PEER REVIEW

The peer review history for this article is available at https://www.webofscience.com/api/gateway/wos/peer-review/10.1111/dom.16309.

DATA AVAILABILITY STATEMENT

The datasets utilized in this study are available in publicly accessible repositories. The specific repository and corresponding accession number are provided here: https://www.ncbi.nlm.nih.gov/, GSE61260, GSE126848 and GSE15653. The raw sequence data reported in this study have been deposited in the Genome Sequence Archive (Genomics, Proteomics & Bioinformatics 2021) in the National Genomics Data Center (Nucleic Acids Res 2022), China National Center for Bioinformation/Beijing Institute of Genomics, Chinese Academy of Sciences (GSA: CRA019010) that are publicly accessible at https://ngdc.cncb.ac.cn/gsa. The data underlying the findings of this study can be obtained from the corresponding author upon reasonable request.

ORCID

Yinxu Fu https://orcid.org/0009-0004-0810-6974
Jianxin Lyu https://orcid.org/0000-0003-2343-1666
Qiongya Zhao https://orcid.org/0000-0001-9616-4787

REFERENCES

1. Perdomo CM, Cohen RV, Sumithran P, Clément K, Frühbeck G. Contemporary medical, device, and surgical therapies for obesity in adults. *Lancet*. 2023;401(10382):1116-1130.
2. Eslam M, Sanyal AJ, George J. MAFLD: a consensus-driven proposed nomenclature for metabolic associated fatty liver disease. *Gastroenterology*. 2020;158(7):1999-2014.e1.
3. Badmus OO, Hillhouse SA, Anderson CD, Hinds TD, Stec DE. Molecular mechanisms of metabolic associated fatty liver disease (MAFLD): functional analysis of lipid metabolism pathways. *Clin Sci Lond*. 2022;136(18):1347-1366.
4. Seo E, Kang H, Choi H, Choi W, Jun HS. Reactive oxygen species-induced changes in glucose and lipid metabolism contribute to the accumulation of cholesterol in the liver during aging. *Aging Cell*. 2019;18(2):e12895.
5. Allameh A, Niayesh-Mehr R, Aliarab A, Sebastiani G, Pantopoulos K. Oxidative stress in liver pathophysiology and disease. *Antioxidants Basel*. 2023;12(9):1653. doi:10.3390/antiox12091653
6. Dong J, Viswanathan S, Adami E, et al. Hepatocyte-specific IL11 cis-signaling drives lipotoxicity and underlies the transition from NAFLD to NASH. *Nat Commun*. 2021;12(1):66.
7. Furman D, Campisi J, Verdin E, et al. Chronic inflammation in the etiology of disease across the life span. *Nat Med*. 2019;25(12):1822-1832.
8. Bala S, Csak T, Saha B, et al. The pro-inflammatory effects of miR-155 promote liver fibrosis and alcohol-induced steatohepatitis. *J Hepatol*. 2016;64(6):1378-1387.
9. Dedemen B, Duman TT, Dedemen MM, Aktas G. Effect of sodium glucose Co-transporter 2 inhibitor use on anthropometric measurements and blood glucose in obese and non-obese type 2 diabetic patients. *Clin Nutr ESPEN*. 2024;63:515-519.
10. Aktas G. Association between the prognostic nutritional index and chronic microvascular complications in patients with type 2 diabetes mellitus. *J Clin Med*. 2023;12(18):5952. doi:10.3390/jcm12185952
11. Kocak MZ, Aktas G, Erkus E, Sincer I, Atak B, Duman T. Serum uric acid to HDL-cholesterol ratio is a strong predictor of metabolic syndrome in type 2 diabetes mellitus. *Rev Assoc Med Bras*. 2019;65(1):9-15.
12. Kosekli MA, Kurtkulagii O, Kahveci G, et al. The association between serum uric acid to high density lipoprotein-cholesterol ratio and non-alcoholic fatty liver disease: the abund study. *Rev Assoc Med Bras*. 2021;67(4):549-554.
13. Hutchins CM, Gorfe AA. From disorder comes function: regulation of small GTPase function by intrinsically disordered lipidated membrane anchor. *Curr Opin Struct Biol*. 2024;87:102869.
14. Zhang L, Cui M, Song L, Zhang M, Zhang J. Function, significance, and regulation of Rap1b in malignancy. *Crit Rev Eukaryot Gene Expr*. 2019;29(2):151-160.
15. Stefanini L, Lee RH, Paul DS, et al. Functional redundancy between RAP1 isoforms in murine platelet production and function. *Blood*. 2018;132(18):1951-1962.
16. Chowdhury CS, Wareham E, Xu J, et al. Rap1b-loss increases neutrophil lactate dehydrogenase activity to enhance neutrophil migration and acute inflammation in vivo. *Front Immunol*. 2022;13:1061544.
17. Sun L, Xie P, Wada J, et al. Rap1b GTPase ameliorates glucose-induced mitochondrial dysfunction. *J Am Soc Nephrol*. 2008;19(12):2293-2301.
18. Xiao L, Zhu X, Yang S, et al. Rap1 ameliorates renal tubular injury in diabetic nephropathy. *Diabetes*. 2014;63(4):1366-1380.
19. Du M, Li X, Xiao F, et al. Serine active site containing protein 1 depletion alters lipid metabolism and protects against high fat diet-induced obesity in mice. *Metabolism*. 2022;134:155244.
20. Tschöp MH, Speakman JR, Arch JR, et al. A guide to analysis of mouse energy metabolism. *Nat Methods*. 2011;9(1):57-63.
21. Horvath S, Erhart W, Brosch M, et al. Obesity accelerates epigenetic aging of human liver. *Proc Natl Acad Sci U S A*. 2014;111(43):15538-15543.
22. Suppli MP, Rigbolt KTG, Veidal SS, et al. Hepatic transcriptome signatures in patients with varying degrees of nonalcoholic fatty liver disease compared with healthy normal-weight individuals. *Am J Physiol Gastrointest Liver Physiol*. 2019;316(4):G462-g472.
23. Pihlajamäki J, Boes T, Kim EY, et al. Thyroid hormone-related regulation of gene expression in human fatty liver. *J Clin Endocrinol Metab*. 2009;94(9):3521-3529.
24. Spitler KM, Shetty SK, Cushing EM, Sylvers-Davie KL, Davies BSJ. Regulation of plasma triglyceride partitioning by adipose-derived ANGPTL4 in mice. *Sci Rep*. 2021;11(1):7873.
25. Piché ME, Tchernof A, Després JP. Obesity phenotypes, diabetes, and cardiovascular diseases. *Circ Res*. 2020;126(11):1477-1500.
26. Fromenty B, Roden M. Mitochondrial alterations in fatty liver diseases. *J Hepatol*. 2023;78(2):415-429.
27. Hoshino A, Kim HS, Bojmar L, et al. Extracellular vesicle and particle biomarkers define multiple human cancers. *Cell*. 2020;182(4):1044-1061.e18.
28. Fan M, Ma X, Wang F, et al. MicroRNA-30b-5p functions as a metastasis suppressor in colorectal cancer by targeting Rap1b. *Cancer Lett*. 2020;477:144-156.
29. Kaneko K, Xu P, Cordonier EL, et al. Neuronal Rap1 regulates energy balance, glucose homeostasis, and leptin actions. *Cell Rep*. 2016;16(11):3003-3015.
30. Chrzanowska-Wodnicka M, Smyth SS, Schoenwaelder SM, Fischer TH, White GC. Rap1b is required for normal platelet function and hemostasis in mice. *J Clin Invest*. 2005;115(3):680-687.
31. Jin J, He Y, Guo J, et al. BACH1 controls hepatic insulin signaling and glucose homeostasis in mice. *Nat Commun*. 2023;14(1):8428.
32. Lu D, He A, Tan M, et al. Liver ACOX1 regulates levels of circulating lipids that promote metabolic health through adipose remodeling. *Nat Commun*. 2024;15(1):4214.
33. Lee H, Lee TJ, Galloway CA, et al. The mitochondrial fusion protein OPA1 is dispensable in the liver and its absence induces mitohormesis to protect liver from drug-induced injury. *Nat Commun*. 2023;14(1):6721.
34. Cheng C, Zhuo S, Zhang B, et al. Treatment implications of natural compounds targeting lipid metabolism in nonalcoholic fatty liver disease, obesity and cancer. *Int J Biol Sci*. 2019;15(8):1654-1663.

35. Liu C, Schönke M, Spoorenberg B, et al. FGF21 protects against hepatic lipotoxicity and macrophage activation to attenuate fibrogenesis in nonalcoholic steatohepatitis. *Elife*. 2023;12:12.

36. Wang Q, Zhou H, Bu Q, et al. Role of XBP1 in regulating the progression of non-alcoholic steatohepatitis. *J Hepatol*. 2022;77(2):312-325.

37. Wang W, Tan J, Liu X, et al. Cytoplasmic endonuclease G promotes nonalcoholic fatty liver disease via mTORC2-AKT-ACLY and endoplasmic reticulum stress. *Nat Commun*. 2023;14(1):6201.

38. Saltiel AR, Olefsky JM. Inflammatory mechanisms linking obesity and metabolic disease. *J Clin Invest*. 2017;127(1):1-4.

39. Govaere O, Petersen SK, Martinez-Lopez N, et al. Macrophage scavenger receptor 1 mediates lipid-induced inflammation in nonalcoholic fatty liver disease. *J Hepatol*. 2022;76(5):1001-1012.

40. Zhang L, Liu M, Liu W, et al. Th17/IL-17 induces endothelial cell senescence via activation of NF-κB/p53/Rb signaling pathway. *Lab Invest*. 2021;101(11):1418-1426.

41. Liu T, Zhang L, Joo D, Sun SC. NF-κB signaling in inflammation. *Signal Transduct Target Ther*. 2017;2:17023-.

42. Oeckinghaus A, Hayden MS, Ghosh S. Crosstalk in NF-κB signaling pathways. *Nat Immunol*. 2011;12(8):695-708.

43. Luedde T, Schwabe RF. NF-κB in the liver--linking injury, fibrosis and hepatocellular carcinoma. *Nat Rev Gastroenterol Hepatol*. 2011;8(2):108-118.

44. Hu J, Wang H, Li X, et al. Fibrinogen-like protein 2 aggravates nonalcoholic steatohepatitis via interaction with TLR4, eliciting inflammation in macrophages and inducing hepatic lipid metabolism disorder. *Theranostics*. 2020;10(21):9702-9720.

45. Gambini J, Stromsnes K. Oxidative stress and inflammation: from mechanisms to therapeutic approaches. *Biomedicines*. 2022;10(4):753. doi:10.3390/biomedicines10040753

46. Ahmed O, Robinson MW, O'Farrelly C. Inflammatory processes in the liver: divergent roles in homeostasis and pathology. *Cell Mol Immunol*. 2021;18(6):1375-1386.

47. Shaikh SR, Beck MA, Alwarawrah Y, MacIver NJ. Emerging mechanisms of obesity-associated immune dysfunction. *Nat Rev Endocrinol*. 2024;20(3):136-148.

48. Bhol NK, Bhanjadeo MM, Singh AK, et al. The interplay between cytokines, inflammation, and antioxidants: mechanistic insights and therapeutic potentials of various antioxidants and anti-cytokine compounds. *Biomed Pharmacother*. 2024;178:117177.

49. Zhang W, Lu J, Feng L, et al. Sonic hedgehog-heat shock protein 90β axis promotes the development of nonalcoholic steatohepatitis in mice. *Nat Commun*. 2024;15(1):1280.

50. Zhao H, Kong L, Shao M, et al. Protective effect of flavonoids extract of Hippophae rhamnoides L. on alcoholic fatty liver disease through regulating intestinal flora and inhibiting TAK1/p38MAPK/p65NF-κB pathway. *J Ethnopharmacol*. 2022;292:115225.

51. Li D, Li Z, Dong L, et al. Coffee prevents IQ-induced liver damage by regulating oxidative stress, inflammation, endoplasmic reticulum stress, autophagy, apoptosis, and the MAPK/NF-κB signaling pathway in zebrafish. *Food Res Int*. 2023;169:112946.

52. Singh AK, Chaube B, Zhang X, et al. Hepatocyte-specific suppression of ANGPTL4 improves obesity-associated diabetes and mitigates atherosclerosis in mice. *J Clin Invest*. 2021;131(17):e140989.

53. Pan X, Shao Y, Wu F, et al. FGF21 prevents angiotensin II-induced hypertension and vascular dysfunction by activation of ACE2/angiotensin-(1–7) Axis in mice. *Cell Metab*. 2018;27(6):1323-1337.e1325.

54. Azzu V, Vacca M, Virtue S, Allison M, Vidal-Puig A. Adipose tissue-liver cross talk in the control of whole-body metabolism: implications in nonalcoholic fatty liver disease. *Gastroenterology*. 2020;158(7):1899-1912.

SUPPORTING INFORMATION

Additional supporting information can be found online in the Supporting Information section at the end of this article.